Asphalt Concrete Fatigue Crack Monitoring and Analysis Using Digital Image Analysis Techniques

Accelerated Pavement Testing 1999 International Conference
October 18-20, 1999
Reno, Nevada

by

Clark Scheffy
University of California at Berkeley
Pavement Research Center
1353 S. 46th St.
Richmond, CA 94804
cscheffy@its.berkeley.edu
Tel: (510) 231-5692
Fax: (510) 231-9589

Ed Diaz
University of California at Berkeley
Pavement Research Center
1353 S. 46th St.
Richmond, CA 94804-4603
Tel: (510) 231-5750
Fax: (510) 231-9589

Paper #CS4-2

INTRODUCTION

The University of California Berkeley Pavement Research Center has been the site for accelerated pavement testing since 1994. Much of the focus of the research has been on fatigue failure of asphalt pavements. As cracking is the visible evidence of fatigue failure, a reliable and consistent method of crack detection and measurement had to be developed. Various methods of digital and manual crack detection and mapping were explored. The method developed and used by the CAL/APT program is described in this paper, and documentation and justification of this process are included. The CAL/APT method employs off-the-shelf software and hardware, making it inexpensive and easy to implement.

In addition, some examples of the analysis of crack data correlation with data obtained from other instruments are presented.

PREVIOUS RESEARCH INTO CRACK DETECTION AND MAPPING AND ITS RELEVANCE TO THE CAL/APT PROJECT

Many researchers have sought to identify methods by which cracks on pavements can be automatically detected and mapped for pavement condition surveys, often with a focus on methods that allow automatic mapping and classification of cracks with equipment moving at highway or near highway speeds (1-3). While this research holds promise for pavement management and maintenance agencies, it is impractical for Heavy Vehicle Simulator (HVS) and similar APT testing frames due to the restricted working space and small pavement area.

Cracks analyzed in the field tend to be pronounced and quite wide due to factors such as exposure to water, thermal effects, and spalling, and fines, making the process of automatically differentiating the cracks from the surrounding pavement relatively easy. Also, in the field, a large sample (multiple kilometers) can be analyzed and, even with a relatively high error rate and low resolution, useful data about the severity of cracking on a field pavement can be obtained.

For HVS test sections, no spalling, thermal effects, moisture effects, or the effects of fines are typically present. The absence of these effects and the fact that the test pavements are trafficked within a year of construction means that the pavement surface stays very dark and that the cracks are too narrow to be detected automatically using any of the currently available equipment and techniques. In addition, the area in which crack data is gathered on an HVS test section measures only 1 x 6 m. For such a small sample, the error rate for automatic mapping would be too high for any useful data to be obtained.

One area of automatic crack detection research that may eventually have applications for APT involves image processing algorithms specifically aimed at detecting thin cracks. Li *et al.* developed an image processing algorithm for thin crack detection and measurement that is capable of detecting cracks less than 0.64 cm wide. (4)

The image processing algorithms used by Li *et al.* rely on differences in luminance, or gray values in the digital image. On a typical pavement, cracks would be darker than the surrounding pavement (i.e., a lower luminance value), and could therefore be differentiated from uncracked pavement. The image processing algorithms presented in Li *et al.* are able to account for noisy images and compensate for anomalous luminance values and thereby detect cracks where many other imaging fail. Such differences are fairly easily detected on field pavements where the pavement surface has lightened due to environmental exposure and aging, and the cracks show up as dark lines relative to the pavement surface. On HVS test sections, the pavement stays very dark and reflective, and differentiating the cracks using luminance values has been thus far impossible.

Li *et al.* also concludes that mapping of “hairline” cracks could be achieved with a higher resolution camera and a smaller field of view. However, the widths of the widest cracks on the CAL/APT HVS test sections have been measured at only 0.2 mm wide. Cracks of this width would require digital image resolution of 10 pixels per square millimeter of pavement surface in order to achieve reasonable automatic crack detection. The equipment (digital or photographic) required to image at this resolution, as well as the number and size of the files required to store and analyze images of such a resolution, make resolution of this magnitude currently impractical.

In Walker and Harris, the use of a laser crack detection system and two data processing algorithms used to locate pavement cracks and filter false cracks were investigated. (5) The researchers concede that for some pavement surfaces (including those with characteristics similar to those of a typical HVS test section), it is doubtful that any filtering algorithm would work well for detecting cracks. The HVS test sections at the Pavement Research Center have all had very shallow, very narrow crack patterns with insufficient relief from the surrounding surface to make laser detection a viable method.

The CAL/APT program found that the most reliable method for imaging and analysis is to identify and mark cracks manually before photographing them. The marks enable the cracks to be easily photographed and traced with image analysis software.

MAPPING CRACKS ON THE CAL/APT TEST SECTIONS

Manual Identification of Cracks

Each CAL/APT HVS test section measures 1 x 8 meters. The sections are marked with paint with index marks at every 0.5 meters along the length of the test area. Each index mark is given a number starting at 0 (e.g., Point 5 on the section would be 2.5 meters from the end).

The Heavy Vehicle Simulator traffics the test section bi-directionally with 1 m of wheel wander. The areas between Point 0 and 2 and between Point 14 and 16 (the first and last meters of the test section) are considered the "turnaround zones." For the purpose of crack mapping, the turnaround zones are ignored so that any effect the changes in speed, loading times, and direction of the test wheel may have on crack growth is not included in the data. The remaining area, or "region of interest," measures 1 x 6 meters, and stretches from Point 2 to Point 14.

Hand-held fluorescent lights are used to illuminate the pavement and groups of three or more technicians lie down on the pavement to search for cracks. All cracks between Point 2 and Point 14 are then marked with a yellow wax lumber crayon. The index points on the pavement are also marked and labeled with the crayon. This process takes approximately one hour.

Imaging of Marked Cracks

The marked pavement is then photographed in 1 x 1 m segments. For the sections discussed in this paper, the camera used was a Pentax 6 x 7 with ISO 400 color film. The camera eyepiece is equipped with a 2x magnifier, which facilitates precise focusing. The camera is positioned approximately 1.2 m above the pavement surface and is attached to the HVS test frame for each image using a clamp with a standard camera mount.

For each 1 x 1 m image, the area of the pavement to be photographed is illuminated with a pair of high-power halogen lights. A single piece of white paper with the number of repetitions and the test section number is placed at the edge of the pavement within the field of view to help identify each image. It was also found that including the piece of white paper helps to set the aperture and shutter speed for the image by providing an appropriate reflective surface for the camera light meter.

Each image includes the index points on either side of the pavement. The camera field of view is roughly oriented to the test pavement edge. Precise orientation of the camera is unimportant because skew and orientation can be corrected digitally in the image analysis software, as described in Section 3.3.2. The exposed film is developed and printed on 4 x 6 in. (10.2 x 15.2 cm) photographic paper.

Note: For sections currently being studied, a Polaroid PDC-3000 digital camera is being used to photograph crack patterns. The digital camera affords several advantages over film for digital analysis. The step of scanning the photographs is eliminated, and cost of the procedure can be reduced because the film development and printing process is eliminated. In addition, the time to develop and process film is eliminated from the procedure.

Mapping the Cracks

Scanning

The resulting prints are scanned into a PC at a resolution of 100 dpi (dots per inch) and saved as TIFF (Tagged Image File Format) files. An example of a scanned file is shown in Figure 1. These images are then opened in photo editing software and cropped to create a set of 12 1 × 0.5 m images, an example of which is shown in Figure 2.

Removing warp and skew

The image files are then opened in Optimas™ where each image is corrected for parallax warp and orientation, as shown in Figure 3. This is done by marking the four corners of each 1 by 0.5 meter pavement area on the source image. Then the coordinates of the desired unskewed image are marked as a 400 by 200 pixel rectangle. [1] The software can then resize and orient the original image to the new coordinates.

Creating the composite image

The properly aligned and unskewed images, each comprising a 0.5-meter length of the test section, are then each opened in a photo editor such as Adobe Photoshop ™ or Corel PhotoPAINT ™. In the graphics editing program, the images are combined on a grid to create a two-dimensional composite image that is 2400 by 400 pixels, as shown in Figure 4. This image is created on a field that is 2500 by 500 pixels so that the test section borders are visible.

Calibrating the image and tracing the cracks

The composite two-dimensional image is then opened in Optimas ™. The first step to perform with the composite image is to calibrate the image dimensions with real-life dimensions. This is done by marking points on the image of known real-life distance, such as the two ends of the section along one 6-meter side. The software then stores the calibration as a ratio of image pixels to a distance on the actual pavement.

The cracks are then manually traced on screen using the computer mouse, as shown in Figure 5.[2] Figure 5 also shows traces from the previous crack set for cumulative crack growth monitoring, as described in Section 3.4. Each crack is marked using a bezier tool (creating straight lines between points on the crack) as continuous until it either terminates or hits another crack or junction.

Extracting the data

After the image is traced, the length and location data is extracted from the image and exported to a spreadsheet file. Optimas™ is configured to extract data in terms of real-life unit samples, which should be no smaller than the ratio of pixels in the image to the real-life units on the pavement section. At the current composite image resolution of 400 pixels/meter, a sample size of 0.25 cm is used. A set of these 0.25 cm samples combine to make crack segments, which are nominally straight portions of a crack. Optimas™ can then output a large number of different measurements. The most useful part of the data is the set of endpoint coordinates for each crack segment. Using this data, crack length for any portion of any crack can be mapped to any grid for correlation of cracking density with other data.

---

[1] It should be noted, in light of the previous discussion of image resolution, that the 400 x 200 pixel rectangle image reduces the resolution, and therefore precision of the resulting image to 0.25 cm/pixel. This is a separate issue from the ability of the imaging equipment to detect the cracks. This resolution is considered precise enough for the desired analyses on the cracked pavement.

[2] Automatic mapping of cracks is possible with Optimas™, and Optimas™ includes the capability to carry out the algorithms and filters used successfully by Li *et al* and discussed in Section 2.1. However, it has been found that automatic identification by this method still produces unacceptable errors on the HVS test pavement.

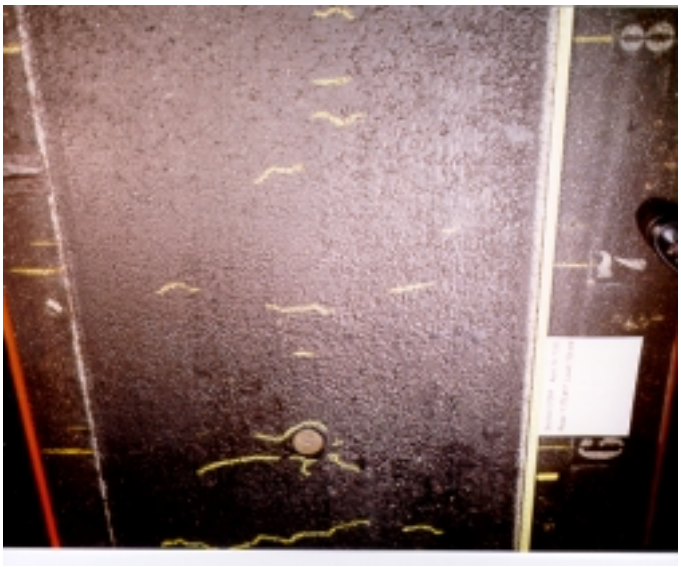

Figure 1. Scanned photograph of 1 x 1 m piece of HVS test section.

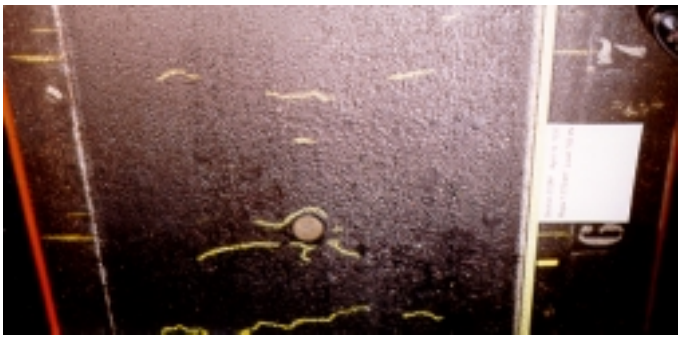

Figure 2. 1 x 0.5 m portion cropped from image of HVS test section.

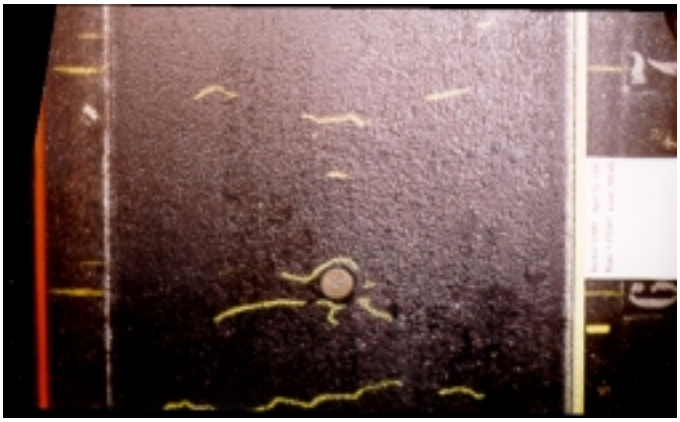

Figure 3. Image from Figure 2 after skew and parallax warp has been removed.

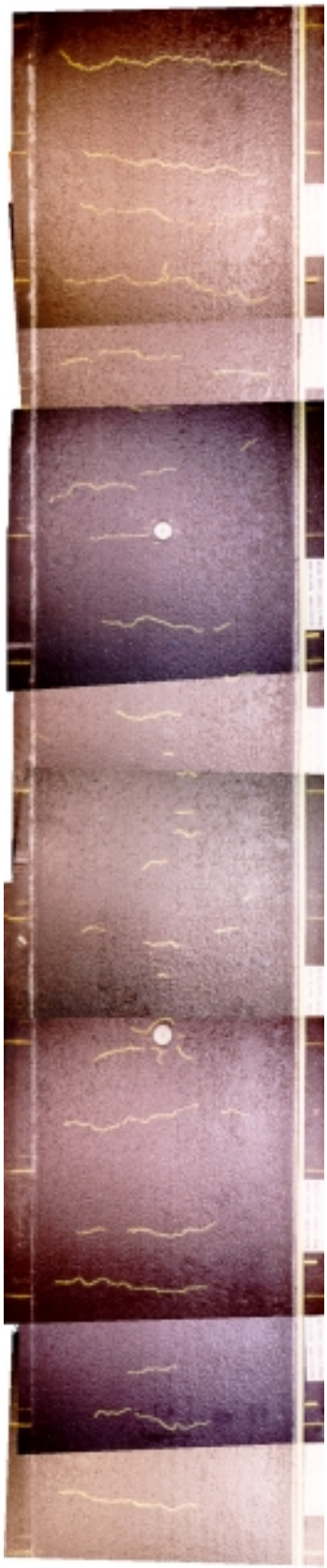

Figure 4. Composite image of HVS test section.

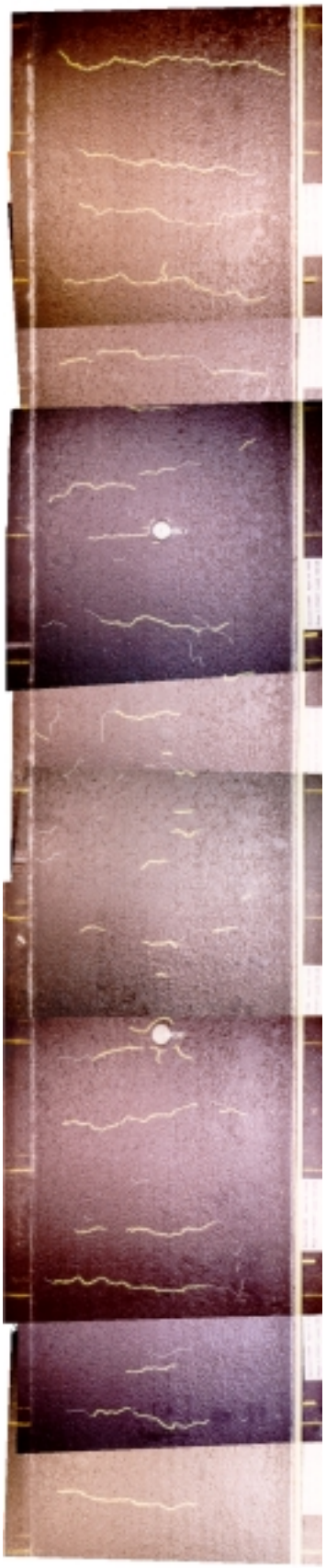

Figure 5. Image from Figure 4 with traced cracks.

Exporting the traced cracks

After the data is extracted, an "overlay" of the cracks is exported as a TIFF file. The overlay is a simple schematic of the traced cracks that can be overlaid on subsequent composite crack images to reduce operator error (Section 3.4).

Cumulative Mapping of Cracks to Compensate for Operator Error

As discussed in Section 2.0, cracks observed on the CAL/APT test sections have been measured to be 0.2 mm wide at the widest points. Such cracks are too narrow to be captured with commercially available imaging equipment without marking the cracks in some way. However, the manual detection and marking method discussed in Section 3.1 has potential for operator error.

Due to operator error, cracks were sometimes not detected during crack data collection. For example, the first set of crack data collected for Section 502 CT showed a reduction in total crack length for the section from 131,000 to 178,000 repetitions.

Some researchers have suggested the possibility of pavement healing as a cause for cracks "disappearing." However, the conditions thought to encourage pavement healing, i.e., temperatures and significant rest periods, were not sufficient to create conditions for significant healing of the test section cracks. (6) Furthermore, cracks that could be visibly detected on the surface of the pavement would not qualify as microcracks, and microcracks are thought to be where pavement healing occurs. (7) Pavement healing was therefore assumed not to occur on the CAL/APT sections, and undetected cracks are assumed to be the result of operator error.

The effect of operator error is reduced by creating cumulative crack maps. The traced cracks from the first composite image for a given test section is overlaid on the composite image of the subsequent image. This allows the operator to both visually check the accuracy of the images as well as trace cracks which may have gone unmarked. It was found that using overlays produced a more reasonable rate of crack growth. It was also found that cracks which had "disappeared" for one set of images would reappear on the subsequent set in the same place.

CORRELATION OF DATA WITH OTHER APT DATA

From the data generated by the crack imaging and mapping method described in this paper, various analyses can be performed. Such analyses include cumulative crack growth with respect to repetitions, crack density mapped over the test section, and the creation of crack pattern schematics. Figure 6 shows the progression of crack growth and the change in the rate of growth for Section 515. Figure 7 shows a schematic of the cracks on Section 515 at the conclusion of the HVS test on that section. Figure 8 shows the density of cracking over Section 515 at the conclusion of the HVS test on that section.

Crack density data can also be correlated to other data for a given test section, such as Falling Weight Deflectometer (FWD) deflections, Road Surface Deflectometer (RSD) deflections, Multi-Depth Deflectometer (MDD) deflections, and nuclear gage density measurements.

For the analyses presented in this section, three test sections were investigated. Section 502 consists of 132 mm of asphalt concrete (AC), 74 mm asphalt-treated permeable base (ATPB), 183 mm aggregate base, and 214 mm aggregate subbase on the subgrade material. Section 503 consists of 131 mm of asphalt concrete (AC), 270 mm of aggregate base, and 303 mm of aggregate subbase on the subgrade material. Section 515 is the overlay of the failed Section 502, and consists of a 36-mm asphalt rubber hot mix (ARHM) overlay on Section 502, with all other design features the same as Section 502. More information on the structure of the sections can be found in the CAL/APT Goal 3 Test Plan. (8)

For each test section, one set of crack data was chosen for comparison with other test data. The crack data sets used were chosen according to the following criteria:

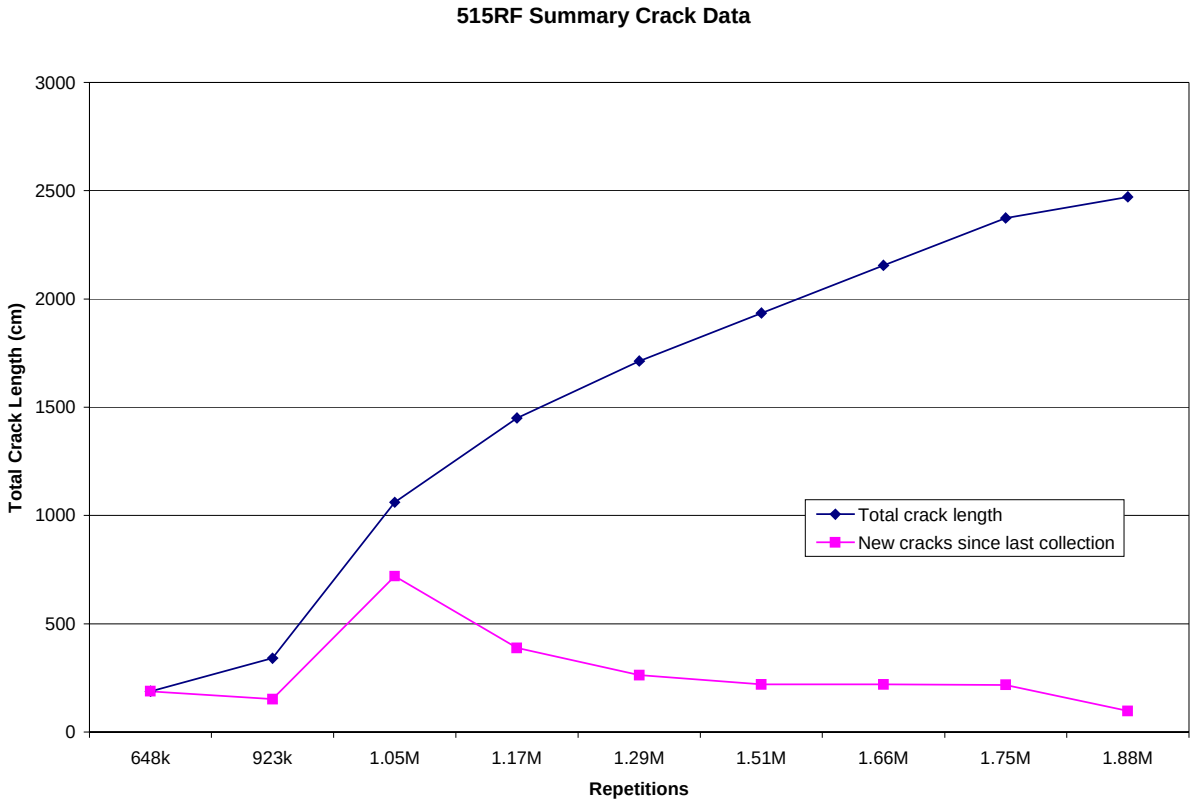

Figure 6. Crack growth with respect to test wheel repetitions, Section 515.

a) the cumulative crack growth had to be at least 1000 cm over the 600 x 100 cm region of interest on the test section in order to provide enough crack data for comparison to other data, and

b) the data set could not be the first set of cracks imaged and mapped from the test section so that the crack data used included multiple images over time and therefore would be less subject to operator error (see Section 4.4).

These criteria led to the choice of the crack data sets shown in Table 1.

For each comparison of crack data and other data presented in the following sections, crack data was obtained for the region of measurement from the other instrumentation with which the crack data was being compared. This was done by obtaining the total crack length (by calculating the hypotenuse of the triangle created by the difference in X

TABLE 1. Summary Data for Crack Data Sets.

Section	Data Set	Repetitions	Total Crack Length for Data Set Used in this Study (cm)	Repetitions at End of HVS Test	Total Crack Length at End of HVS Test (cm)	Cracking Density at End of HVS Test (cm/cm^2)
502	4	2094873	1000.75	2673589	2394.75	0.040
503	2	910000	1628.75	1911823	3909.50	0.052
515	3	1054099	1061.50	1885637	2470.50	0.041

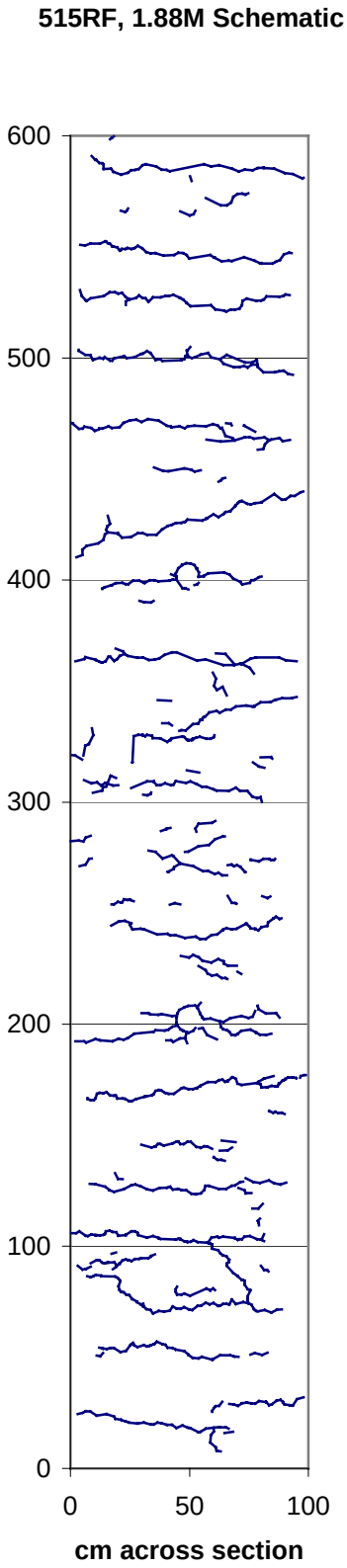

Figure 7. Crack schematic, Section 515.

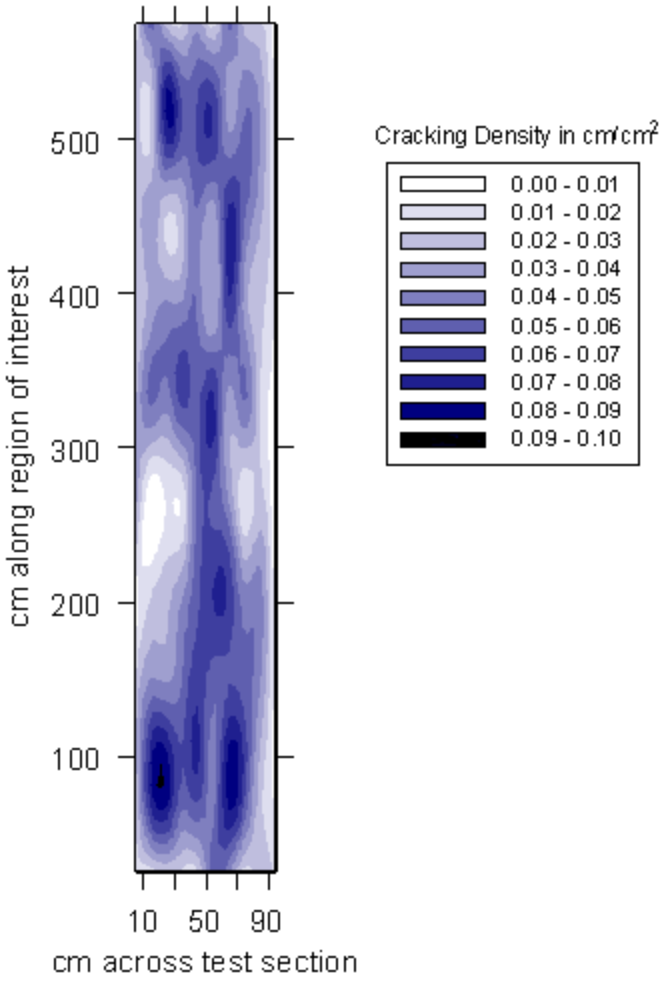

Figure 8. Contour map of cracking density, Section 515.

and difference in Y between the endpoints of the crack segment) for each crack segment that fell within the measurement region. The total crack length for the measurement region was then divided by the area of the region to obtain cracking density.

Effect of HVS Test Wheel Wander of Crack Location

Load repetitions are the principle cause for crack development, and the most significant factor affecting crack location and density is the number of actual repetitions experienced by various portions of an HVS test section. When the HVS is set to traffic with sideshift (to simulate traffic wander), the longitudinal center of the HVS test section receives almost three times as many repetitions as each of the outside regions of the test section. For a given number of HVS repetitions, 64 percent are delivered to the center 28 cm strip of the test section. 46 percent of the repetitions are divided among the two outer 36 cm strips, resulting in 23 percent of the repetitions being delivered to each of the side regions of the test section. (9) (Note that these percentages are for wheel passes, not wheel coverage, hence a total percentage greater than 100.) For this reason, cracks are expected to first appear along the center of the test section. Figure 9 shows the three regions on an HVS test section.

Crack data for all three test sections included in this study was mapped to these regions to compare cracking density with respect to actual traffic repetitions in an HVS test with simulated traffic wander, as shown in Table 2.

As is evident from the data presented in Table 2, the center region of each test section shows considerably higher cracking density than the side portions.

TABLE 2. Cracking Density with respect to Traffic Wander.

Section	Region	Share of Repetitions (Percent)	Total Crack Length (cm)	Region Dimensions (cm^2)	Cracking Density (cm/cm^2)
502	Sides	23	520.9	43,200	0.012
	Center	54	449.5	16,800	0.027
503	Sides	23	998.8	43,200	0.023
	Center	54	595.0	16,800	0.035
515	Sides	23	576.7	43,200	0.013
	Center	54	484.7	16,800	0.029

Multi-Depth Deflectometers (MDDs)

Multi-Depth Deflectometers are installed on all HVS test sections to measure deflections and permanent deformation in each pavement layer over the life of each test section. The MDDs measure deflections at various layers within the pavement structure. The MDD data from Sections 502, 503, and 515 were compared with crack data for those sections. Figure 10 shows the location of the MDDs and the areas in which crack density was mapped for Sections 502 and 503; Figure 11 shows the location of the MDDs and the areas in which crack density was mapped for Section 515.

The mapped regions were centered on the MDD locations and limited in the transverse direction to the 28 cm “center region” determined by the wander of the test wheel, as described in Section 4.1. The regions were arbitrarily limited in the longitudinal direction to 50 cm. It is not known at this time whether the longitudinal dimension of 50 cm is appropriate, and further study into the influence of the test wheel is required.

Table 3 shows the results of the comparison of crack data and MDD data for Sections 502, 503, and 515. A 100kN load was used to obtain the deflections for each section. The first MDD data set taken at 100kN for each test section was used for this study. In all except MDD 4 on Section 503, the surface deflection data had to be extrapolated from the MDD data at underlying layers. From Table 3, it can be seen that higher cracking density is evident in regions with higher measured MDD deflections.

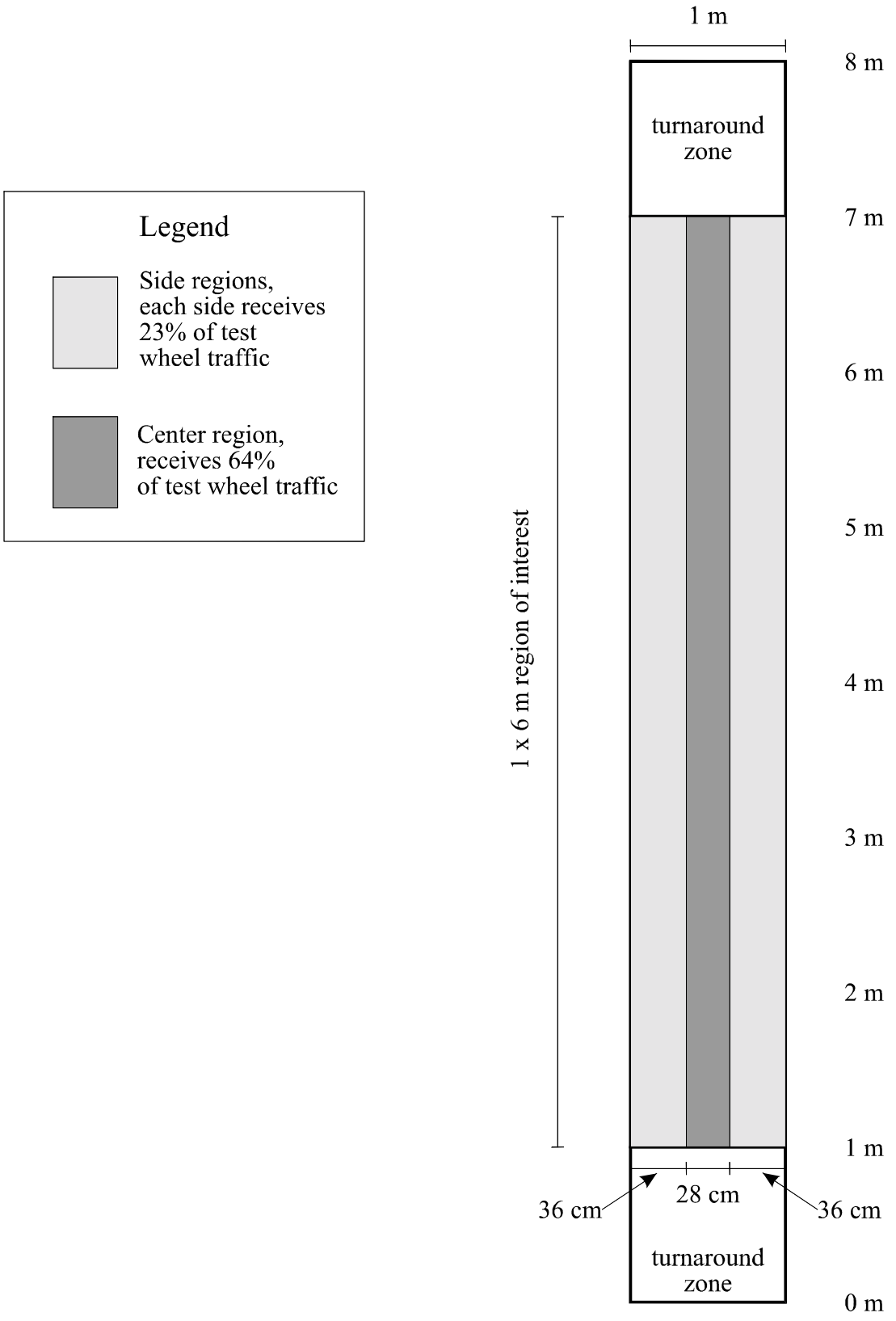

Figure 9. Location of traffic wander regions on HVS test sections.

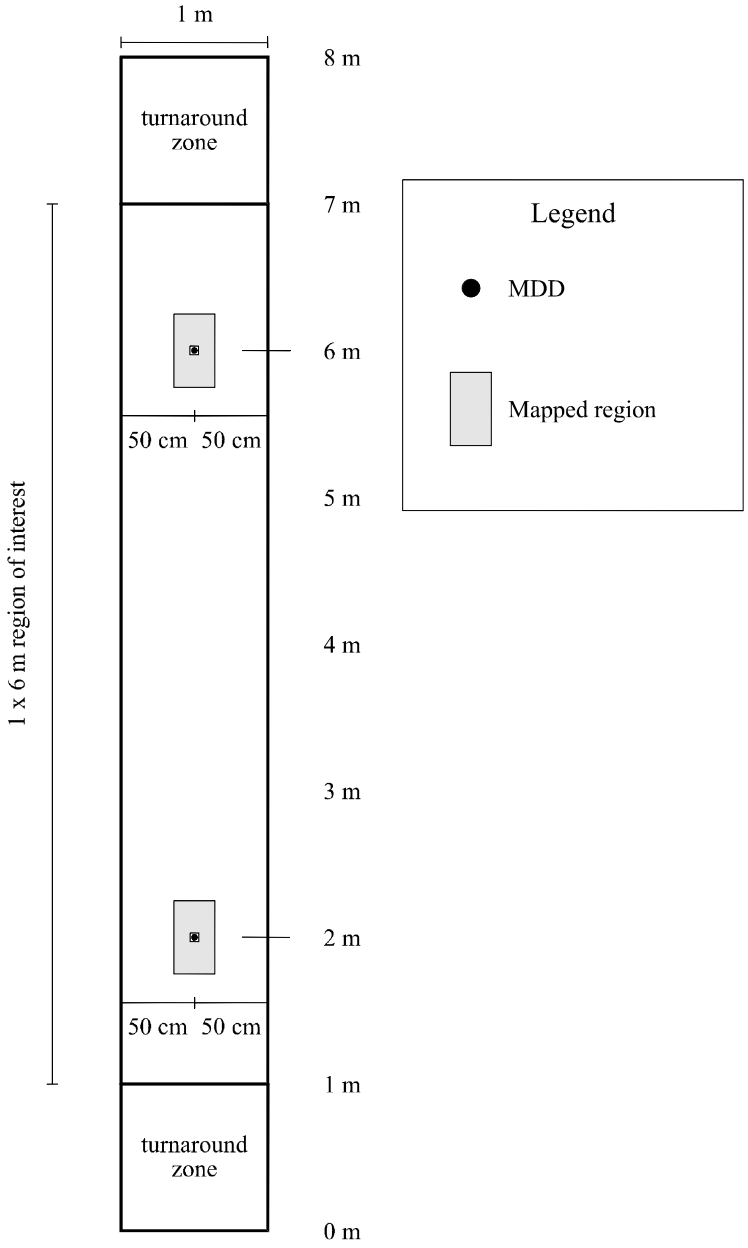

Figure 10. Locations of MDDs and mapped regions on Sections 502 and 503.

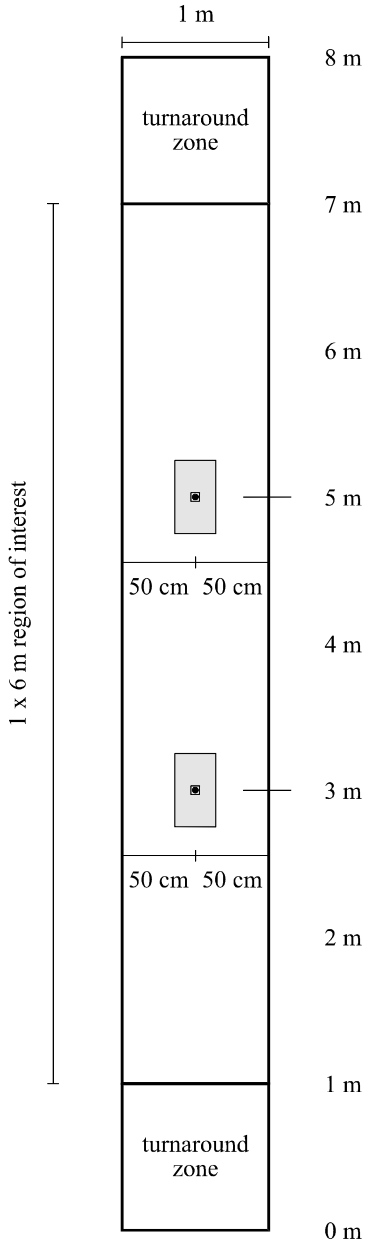

Figure 11. Locations of MDDs and mapped regions on Section 515.

TABLE 3. Cracking Density with respect to Deflections Measured by Multi-Depth Deflectometers, 100kN Load.

Section	MDD location (m from end of section)	Repetitions at time of MDD data collection	Crack Length (cm)	Mapped area (cm^2)	R-squared for Surface Deflections	Surface Deflections ($mm \times 10^{-3}$)	Cracking Density (cm/cm^2)
502	2	192616	28.80	1400	0.97	695	0.0206
	6	192616	31.64	1400	0.99	964	0.0226
503	2	199958	36.66	1400	*real value used*	871	0.0262
	6	199958	53.24	1400	0.98	1145	0.0380
515	3	346333	23.08	1400	0.96	1072	0.0165
	5	346333	8.63	1400	0.87	728	0.0062

RSD

The Road Surface Deflectometer is essentially a modified Benkelman beam. The beam has a measurement end that passes between the dual tires of the HVS test wheel and a reference end. An LVDT measures the deflection 1/3 the way from the reference point. A diagram of the RSD measurement locations is shown in Figure 12.

Road Surface Deflectometer measurements were made at regular intervals during the HVS trafficking of Sections 502, 503, and 515. For each test section, the data used was the first set of deflection data obtained at a load of 100kN and which included RSD points along the centerline of the test section as well as 200 mm off-center on either side. For the centerline set of RSD measurements, the mapped regions were centered on the RSD locations and limited in the transverse direction to the 28 cm "center region" determined by the wander of the test wheel, as described in Section 4.1. For the side RSD measurements, the mapped regions were centered on the RSD locations and limited in the transverse direction to 12 cm in order to stay within the "side region" determined by the wander of the test wheel. The regions were arbitrarily limited in the longitudinal direction to 50 cm. It is not known at this time whether the longitudinal dimension of 50 cm is appropriate, and further study into the influence of the test wheel is required. Table 4 presents a comparison of RSD deflections and crack density data.

From Table 4, it can be seen that increased cracking density is evident in all the regions with increased surface deflections except for the side regions on Section 515. The reason for the inconsistency on Section 515 is not known at this time. It is possible that operator error caused a crack to go undetected. Visual inspection of crack schematics for Section 515 suggest that segments of some cracks were not detected visually in a region of high RSD deflections in the data set considered for this study, and were detected visually (the crack segments joined together) in subsequent data sets. The undetected crack in the area of high deflection may be the cause for the inconsistency in the data presented.

FWD

Dynatest Consulting of Ojai, California performed a series of falling weight deflectometer (FWD) tests on the aggregate base and the asphalt concrete comprising the HVS test pavements at the Richmond Field Station. The first sets of tests were used to locate areas with reasonably consistent and similar stiffness, which could then become the HVS test sections.

Dynatest conducted another series of FWD tests with test points every foot along the centerline of the HVS test sections after the sections were considered failed. The surface deflection data from this series of tests were examined to determine if any correlation existed between locations of high FWD deflections and crack formation. The mapped regions were centered on the FWD test point locations and were limited in the transverse direction to the 28 cm "center region" determined by the wander of the test wheel, as described in Section 4.1. The regions of

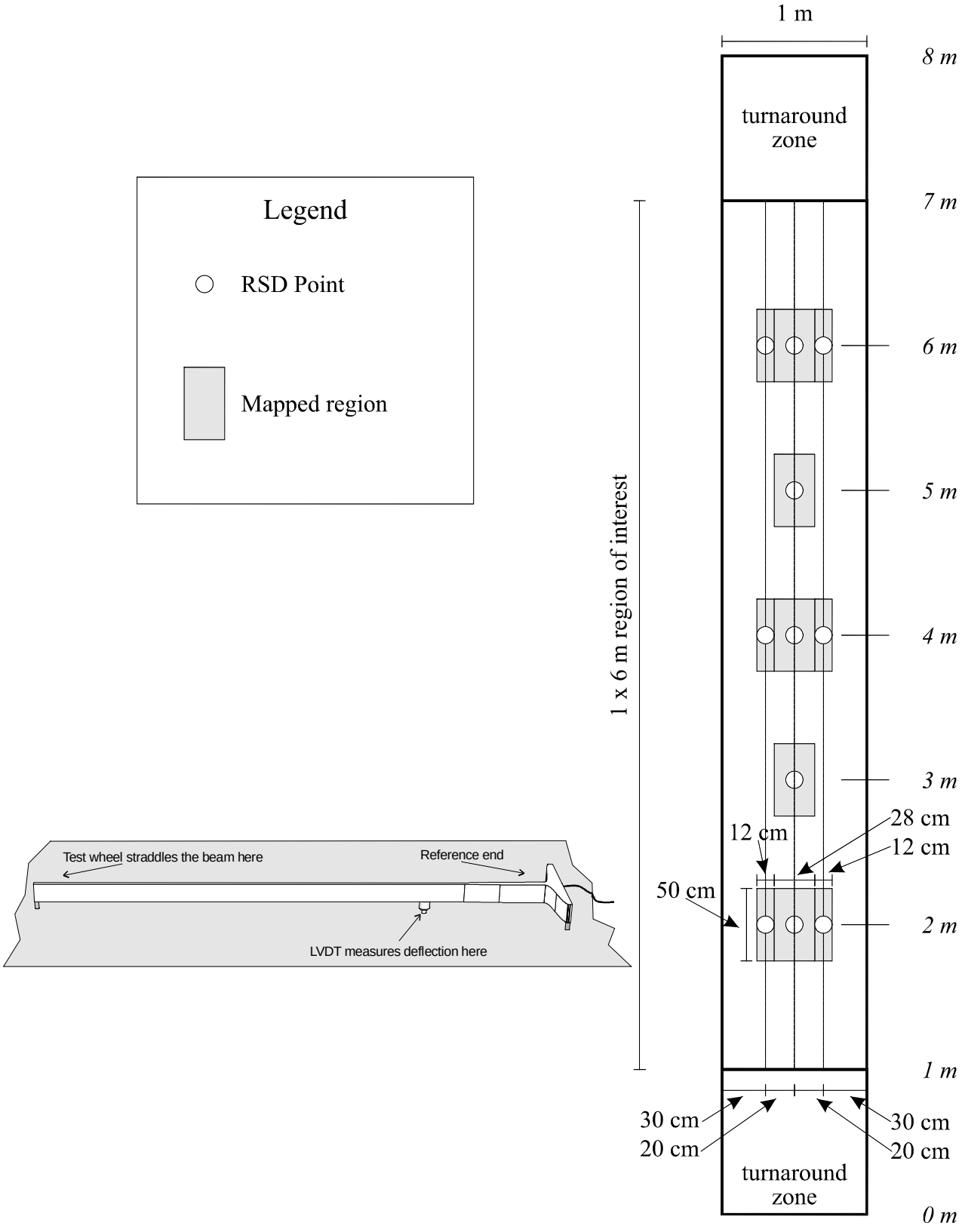

Figure 12. Location of RSD measurement points and mapped regions on HVS test sections.

measurement were limited in the longitudinal direction to 30.5 cm. The FWD test point locations and regions of measurement for Sections 502 and 503 are shown in Figure 13.

The FWD data used was collected on October 9, 1996, after the trafficking on Sections 502 and 503 had concluded. The FWD data used for comparison to crack data was the "high stress" set with deflections measured at the closest geophone. Table 5 presents a comparison of FWD deflections and cracking density to show the relationship of relative FWD deflections to cracking density. From Table 5, it can be seen that increased cracking density is evident in regions with increased FWD deflections.

Nuclear Gage

Nuclear gages were regularly used on the HVS test sections to measure change in density of the asphalt concrete layer with respect to HVS repetitions. The measurements were made nondestructively with the gage in backscatter mode. Measurement points are shown in Figures 14 and 15 for Sections 502-503 and 515, respectively.

The first set of nuclear gage measurements taken on each of the sections were used for this study. For Section 515,

TABLE 4. Cracking Density with respect to Deflections Measured by Road Surface Deflectometer, 100 kN Load.

Section	Repetitions at RSD Data Collection	Region	Mean Surface Deflections (mm)	Average Cracking Density (cm/cm^2)	
502	192616	Centerline	852.9	< Mean Deflection	0.017
				> Mean Deflection	0.019
		Sides	962.2	< Mean Deflection	0.015
				> Mean Deflection	0.018
503	199958	Centerline	882.2	< Mean Deflection	0.024
				> Mean Deflection	0.030
		Sides	861.1	< Mean Deflection	0.027
				> Mean Deflection	0.045
515	346333	Centerline	1151.8	< Mean Deflection	0.017
				> Mean Deflection	0.026
		Sides	1070.9	< Mean Deflection	0.018
				> Mean Deflection	0.000

TABLE 5. Cracking Density with respect to Deflections Measured by Falling Weight Deflectometer.

Section	Mean FWD Stress (kPa)	Mean Surface Deflection (mm)	Cracking Density (cm/cm^2)	
502	853	383.8	< Mean Deflection	0.015
			> Mean Deflection	0.035
503	844	637.4	< Mean Deflection	0.030
			> Mean Deflection	0.045

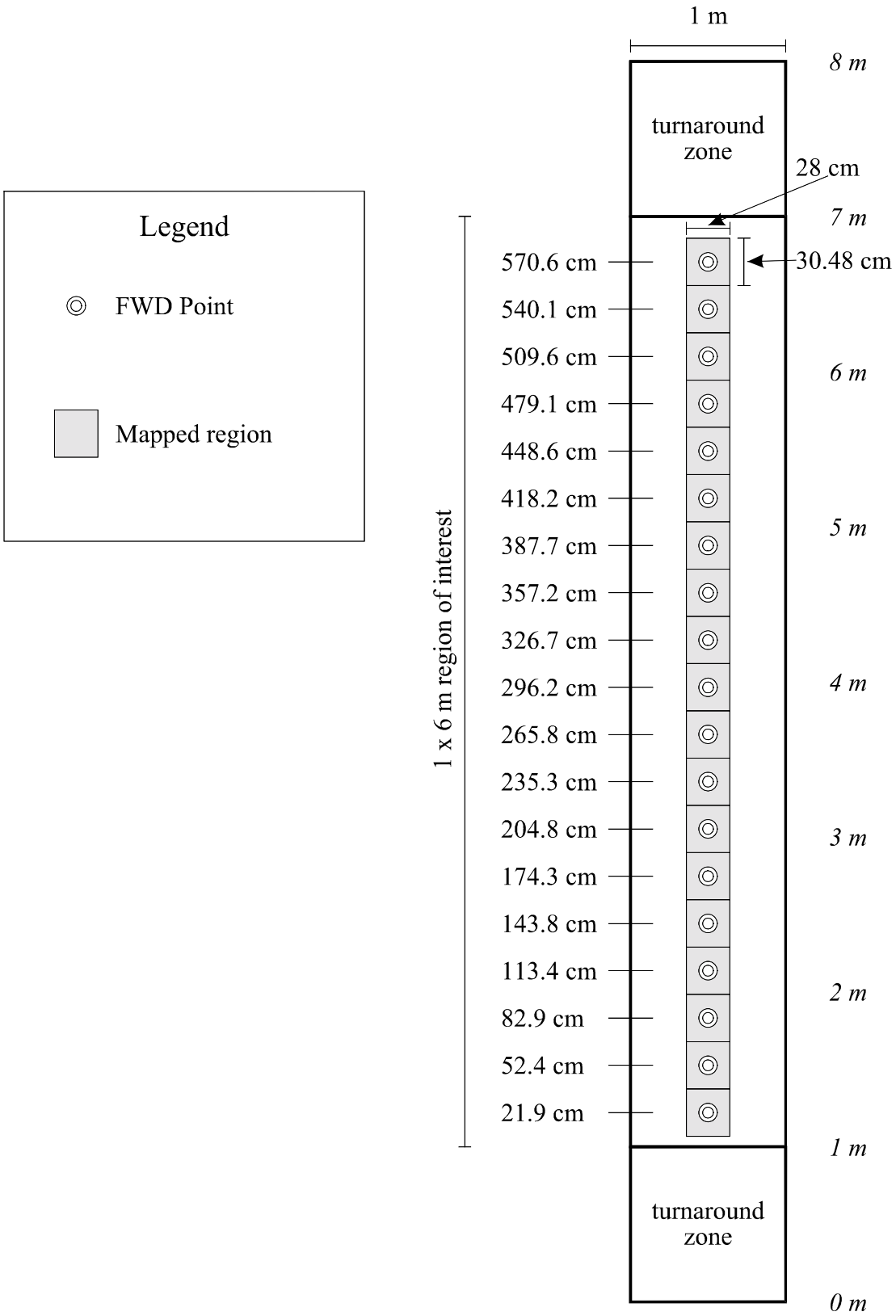

Figure 13. Location of FWD measurement points and mapped regions on HVS test sections.

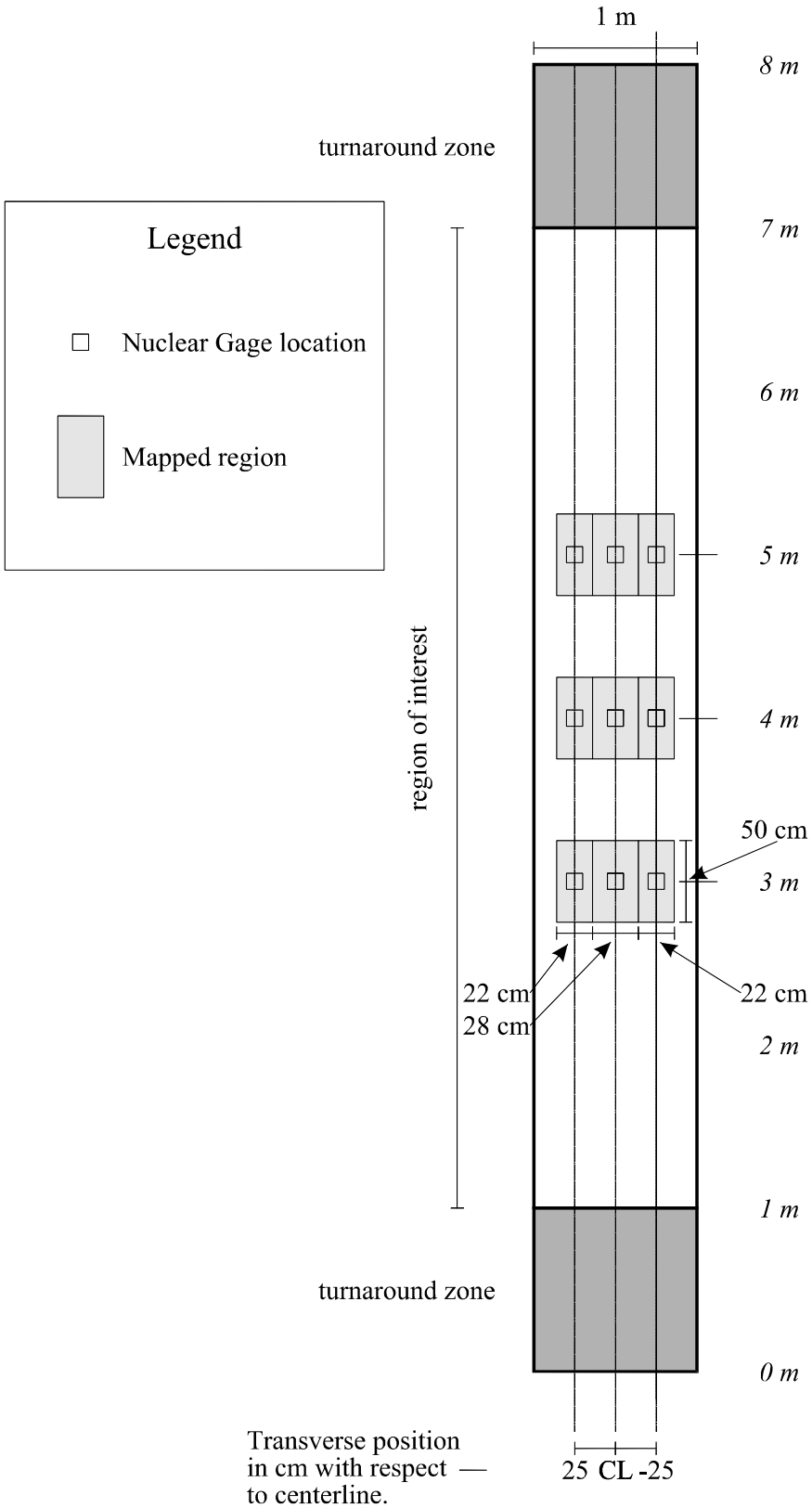

Figure 14. Locations of nuclear gage measurement points and mapped regions on HVS Sections 502 and 503.

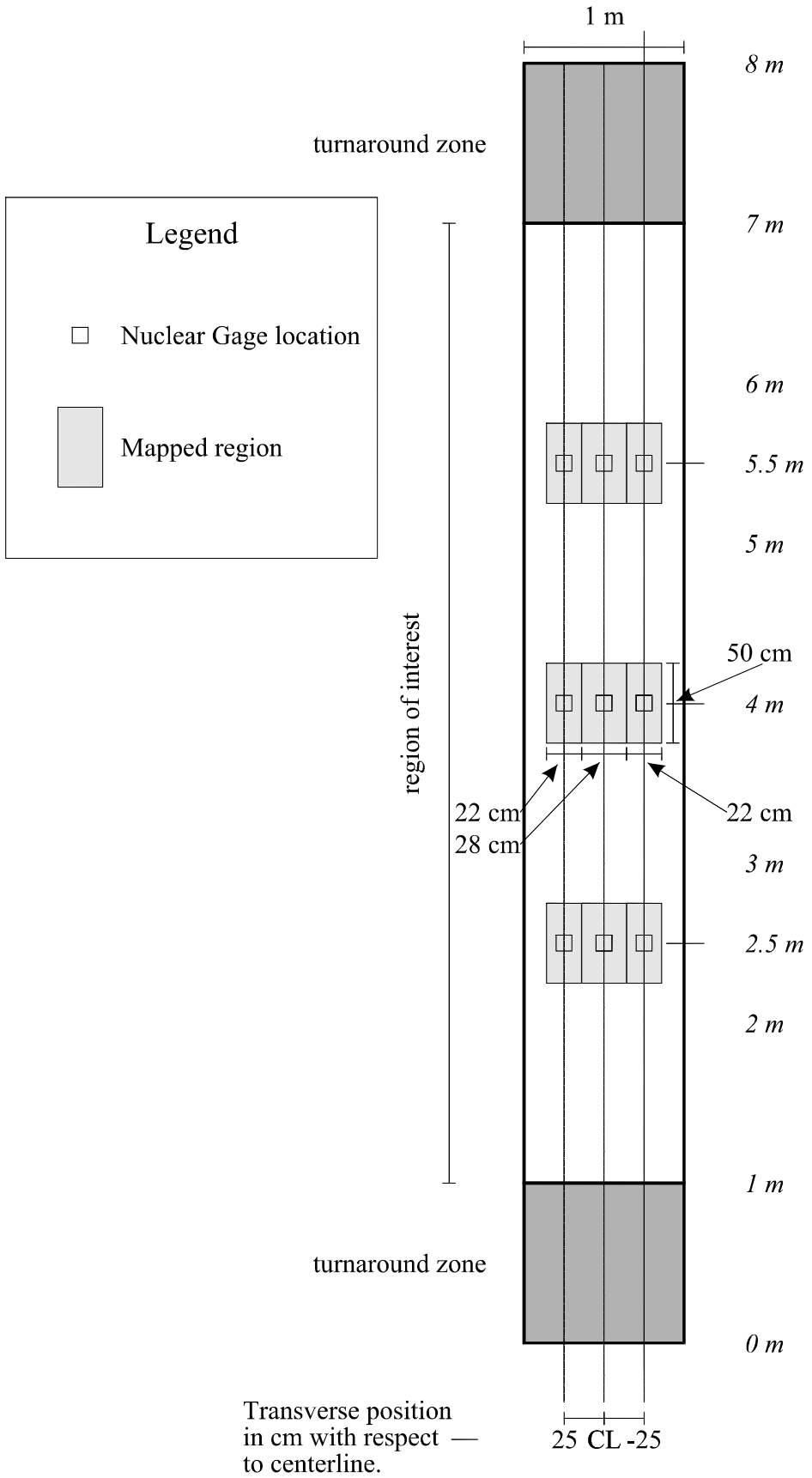

Figure 15. Location of nuclear gage measurement points and mapped regions on HVS Section 515.

the nuclear gage measurements were taken before any HVS trafficking began. For Sections 502 and 503, nuclear gage readings were not made prior to the start of HVS testing, and the nuclear gage AC densities are affected by the deformation caused by HVS trafficking. However, it is assumed that the first set of nuclear gage readings on both Sections 502 and 503 gives an acceptable indication of relative densities across the test section, and therefore can still indicate the relationship between nuclear gage density measurements and cracking density.

Table 6 presents a comparison of nuclear gage density measurements (converted to air-voids) and cracking density. From Table 6, it can be seen that for all but the side regions of Section 502, increased cracking density is evident in areas with increased air-voids.

SHORT INVESTIGATION OF REFLECTION CRACKING

The crack analysis and mapping techniques presented in this paper have also confirmed the phenomenon of reflection cracking on Section 515, which is the overlay of Section 502. Crack schematics of both sections are combined and shown in Figure 16.

From the figure is can be seen that cracks on the overlay section (Section 515) in many cases appear in exactly the same place as cracks on the underlying cracked section (Section 502).

TABLE 6. Cracking Density with respect to Pavement Density (Air-Voids) Measured by Nuclear Gage.

Section	Repetitions at Nuclear Gage Data Collection	Region	Mean Air-Voids[1]	Average Cracking Density (cm/cm^2)	
502	650404	Centerline	4.17	< Mean Air-Voids	0.013
				> Mean Air-Voids	0.021
		Sides	4.47	< Mean Air-Voids	0.004
				> Mean Air-Voids	0.004
503	412000	Centerline	4.23	< Mean Air-Voids	0.022
				> Mean Air-Voids	0.023
		Sides	4.27	< Mean Air-Voids	0.005
				> Mean Air-Voids	0.019
515	0	Centerline	9.48	< Mean Air-Voids	0.027
				> Mean Air-Voids	0.034
		Sides	8.67	< Mean Air-Voids	0.013
				> Mean Air-Voids	0.021

1) It should be noted that the air-voids shown in the table are derived from nuclear gage measurements, and in the case of Sections 502 and 503, the air-voids have been shifted to more closely match laboratory air-voids measurements. The purpose of showing air-voids is to demonstrate the effect of relative compaction on crack development.

CONCLUSION

Much research has been done in the field of automated crack imaging and mapping, but this research is not yet applicable to the particular characteristics of accelerated pavement testing with the Heavy Vehicle Simulator (HVS). The method developed by the CAL/APT program is easy to perform and efforts have been made to reduce the effects of operator error on the results obtained with the method.

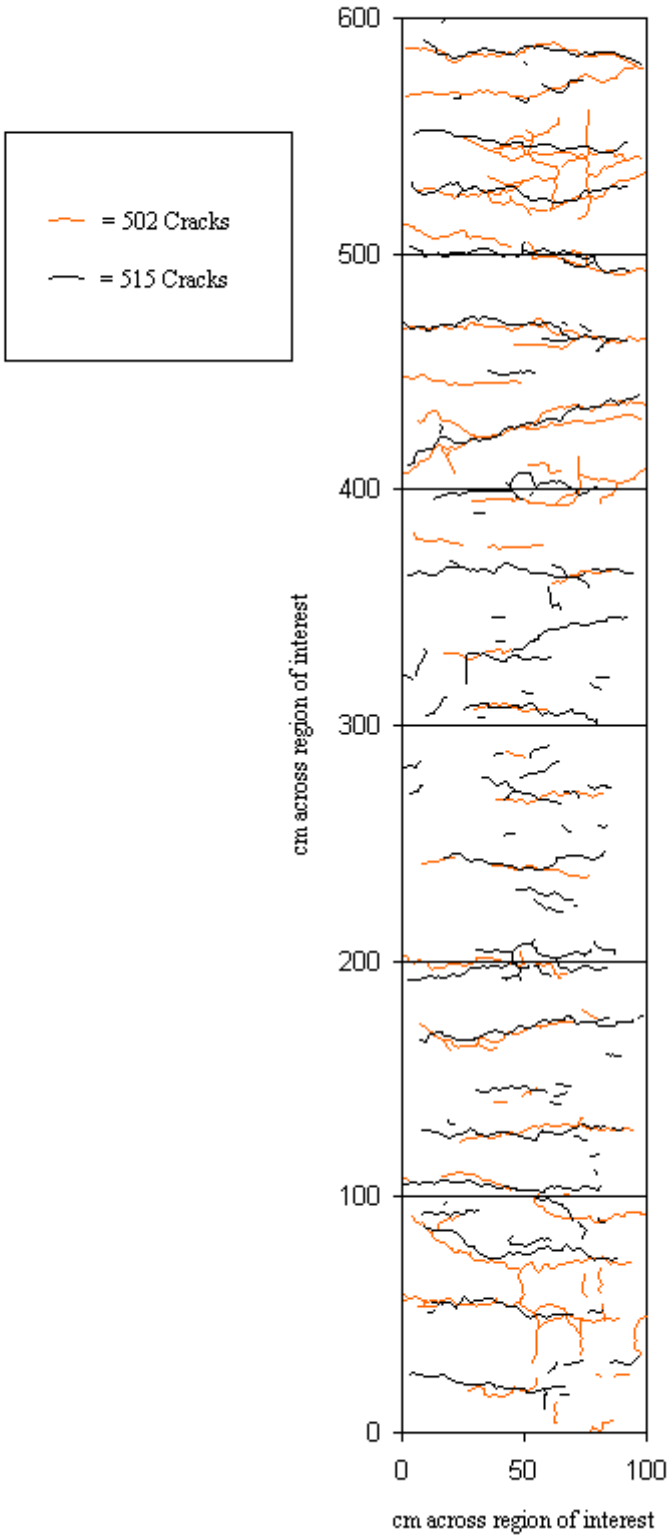

Figure 16. Crack schematics from underlying (Section 502) and overlay (Section 515) superimposed to demonstrated reflection cracking.

Data obtained from crack imaging and mapping using the method described herein can be correlated to other test section data as long as the location on the test section for other data is known. Deflection data, density (air voids) data, and traffic wander data can all be related to cracking density. In addition, reflection cracking can be mapped and demonstrated to occur in asphalt concrete overlays.

Further research is required to find better methods for imaging cracked sections, including the use of digital cameras or related equipment and automated crack mapping with the goal of greater accuracy and reduced operator error. Further use of the method to study reflection cracking is also suggested.

This paper did not present statistical analyses of any of the data correlation. The goal of the research was limited to demonstrating the concept of correlating data from various instruments to the data obtained from the CAL/APT crack imaging and mapping technique.

REFERENCES

1. H. N. Koutsopoulos and I El Sanhouri. 1991. Methods and Algorithms for Automated Analysis of Pavement Images. *Transportation Research Record 1311,* TRB, National Research Council, Washington, D.C., pp. 103-111.

2. S. G. Ritchie, M. Kaseko, and B Bavarian. Development of an Intelligent System for Automated Pavement Evaluation. 1991. *Transportation Research Record 1311,* TRB, National Research Council, Washington, D.C., pp. 112-119.

3. M. H. Mohajeri and P. J. Manning. ARIA™: An Operating System of Pavement Distress Diagnosis by Image Processing. 1991. *Transportation Research Record 1311,* TRB, National Research Council, Washington, D.C., pp. 120-130.

4. L. Li, P. Chan, and R. L. Lytton. Detection of Thin Cracks on Noisy Pavement Images. 1991. *Transportation Research Record 1311,* TRB, National Research Council, Washington, D.C., pp. 131-135.

5. R. S. Walker and R. L. Harris. 1991. Noncontact Pavement Crack Detection System. *Transportation Research Record 1311,* TRB, National Research Council, Washington, D.C., pp. 149-157.

6. Kim, Y. Richard; Little, Dallas N.; Benson, Fred C. 1990. Chemical and Mechanical Evaluation on Healing Mechanism of Asphalt Concrete. *Journal of the Association of Asphalt Paving Technologists,* Vol. 59, pp. 240-272.

7. Kim, Y. R.; Whitmoyer, S.L.; and Little, D. N. 1994. Healing in Asphalt Concrete Pavements: Is it Real? *Transportation Research Record 1454,* TRB, National Research Council, Washington D.C., pp. 89-96.

8. Dynatest Consulting, Inc., University of California, Berkeley, and Division of Roads and Transport Technology, CSIR. 1997. Test Plan for CAL/APT Goal 3. Report delivered to California Department of Transportation. March 1997.

9. Harvey, J. T., du Plessis, L., Long, F., Deacon, J. A., Guada, I. M., Hung, D., Scheffy, C. 1997. CAL/APT Program: Test Results from Accelerated Pavement Test on Structure Containing Asphalt Treated Permeable Base (ATPB)—Section 500RF.